

# Experimental and Numerical Heat Transfer from Vortex-Injection Interaction in Scramjet Flowfields

Juan R. Llobet<sup>1</sup>, Kevin D. Basore<sup>2</sup>, Rowan J. Gollan<sup>3</sup> and Ingo H. Jahn<sup>4</sup>

*University of Queensland, Brisbane, QLD 4072, Australia*

Air-breathing propulsion is expected to decrease the cost per kilogram for access-to-space, while increasing the flexibility of available low earth orbits. However, improvements are required in order make this a reality, with one of the current issues under investigation being the effective fuel-air mixing inside of scramjet engines. A viable option suggested to address this issue uses the intrinsically generated vortices from scramjet inlets to enhance fuel-air mixing further downstream. Previous works have studied this vortex-injection interaction numerically, but the lack of published experimental data in the hypersonic regime make validation impractical. This paper extends upon these previous works by providing experimental data for a canonical geometry and assessing the accuracy of the numerical methodology to predict the vortex-injection interaction.

To achieve this, an experimental model consisting of a flat plate with a perpendicular compression fin and a porthole injector is tested in the T4 Stalker Tube. The experimental data is replicated numerically, allowing for the validation of the numerical methods. These results show a localized overprediction of the heat transfer, attributed to a localized overprediction of the turbulent kinetic energy. Nonetheless, a good agreement was seen overall between the numerical and experimental results.

---

<sup>1</sup> PhD candidate, Centre for Hypersonics, School of Mechanical and Mining Engineering, j.r.llobet@uq.edu.au, Student Member AIAA.

<sup>2</sup> PhD candidate, Centre for Hypersonics, School of Mechanical and Mining Engineering, k.basore@uq.edu.au, Student Member AIAA.

<sup>3</sup> Lecturer, Centre for Hypersonics, School of Mechanical and Mining Engineering, r.gollan@uq.edu.au, Member AIAA.

<sup>4</sup> Lecturer, Centre for Hypersonics, School of Mechanical and Mining Engineering, i.jahn@uq.edu.au, Member AIAA.

*COMMENT IJ: The abstract fails to capture the heat transfer aspect of the paper. Knowing heat transfer, so that appropriate thermal management startegies can be applied is equally important.*

### Nomenclature

$\varnothing$  = Diameter [mm]

$\alpha_{fin}$  = Fin angle [deg]

$\alpha_R$  = TFHG sensitivity [ $K^{-1}$ ]

$\delta$  = Boundary layer thickness [mm]

$\rho$  = Density [ $kg\ m^{-3}$ ]

$c$  = Thermal capacity [ $J\ kg^{-1}\ K$ ]

$H$  = Enthalpy [ $MJ\ kg^{-1}$ ]

$k_T$  = Thermal conductivity [ $W\ m^{-1}\ K$ ]

$M$  = Mach number [-]

$P$  = Pressure [Pa]

$q, Q$  = Heat flux [k/watt/per/square/meter]

$t$  = Time [s]

$T$  = Temperature [K]

$u$  = Velocity [ $m\ s^{-1}$ ]

$V$  = Voltage [V]

## I. Introduction

By removing the requirement of having to carry the propellant oxidizer, air-breathing propulsion has significant theoretical advantages over rockets. These advantages include, a higher specific impulse, efficiency, and payload mass fraction [1, 2]. For these reasons, using air-breathing propulsion for access-to-space missions has the potential to increase the overall efficiency as well as decrease the cost per kilogram of placing satellites into orbit. However, several aspects of scramjet technology still require substantial improvements prior to scramjet propulsion for access-to-space being considered

operational. The extremely short residence times to mix and burn the fuel within these engines is one of the main challenges. A previously suggested strategy to enhance mixing while incurring a minimal total loss increase, is to use the vortices intrinsically generated by scramjet inlets. Non-axisymmetric inlets inherently generate vortices due to the presence of Shock-Wave Boundary-Layer Interactions (SWBLI) [3]. These vortices have been shown to produce improvements in mixing [4, 5]. Llobet et al. [5] shows, using a Reynolds Averaged Navier-Stokes (RANS) Computational Fluid Dynamics (CFD) study, that by injecting into a representative inlet sidewall SWBLI vortex, the air-fuel mixing rate was substantially improved. The vortices in this study were generated using a canonical geometry consisting of a flat plate and a compression wall, which is shown to generate vortices representative of those found in scramjet flowfields [6]. This geometry is replicated in the current experiment to provide experimental data as a validation benchmark against the numerical studies previously published on this topic. The experiments were carried out in the T4 Stalker Tube at the University of Queensland (UQ).

## II. T4 Reflected Shock Tunnel

The T4 Stalker Tube is a free-piston reflected shock tube at the University of Queensland. Commissioned in 1987 [7] from the design of Stalker [8], the tunnel is capable of a total enthalpy range of 3-15 MJ/kg [7] at a variety of Mach numbers [9]. This high-enthalpy impulse facility is usually run in a direct connect [10, 11] or semi free-jet configuration [12, 13] due to the relatively small core size of the facility [14, 15].

Able to achieve test times on the order of 1 ms [14], this facility has been used extensively for scramjet propulsion/high-speed aerodynamic research [16, 17]. Figure 1 shows a generic overview of the facility with reference [7] containing an extensive description of the facility for the interested reader.

## III. Experimental Model

Figure 2 shows the simplified geometry, consisting of a flat plate and a normal fin at an angle of attack used to generate scramjet-inlet like vortices. The resulting flowfield, with the freestream velocity moving in the positive x direction, generates a vortex through shock-viscous interactions,

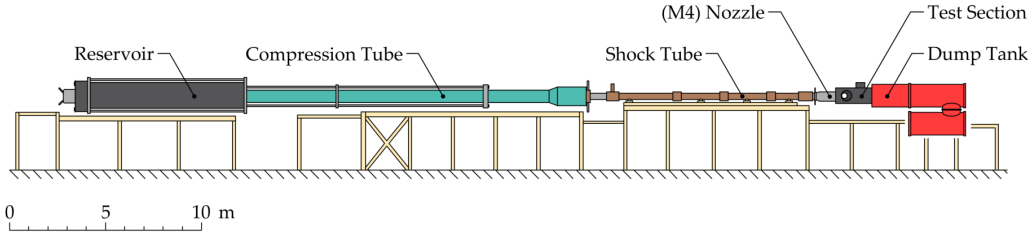


Fig. 1: A generic overview of the T4 Stalker Tube. Extracted from [7].

which is similar to the vortices generated by non-axisymmetric scramjet inlets [5, 6].

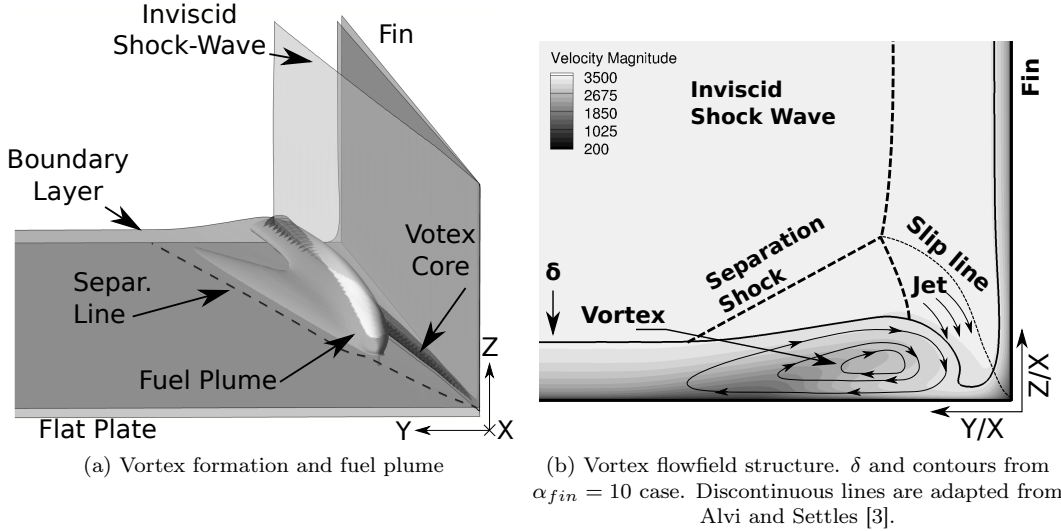


Fig. 2: Test geometry and vortex flowfield structure depiction. Extracted from [18]

Figure 3 shows the corresponding model used in the experimental campaign. For the experiment the fin angle was set at  $10^\circ$ . This angle was chosen due to the relative strength of the generated vortex being representative of vortices present in previously tested engines [4, 6].

The width of the model/plate is 220 mm, which was selected to reduce the potential of any three-dimensional effects contaminating the measurement area. The length of flat plate upstream of the fin leading edge is limited to 156 mm due to the potential interference with the tunnel nozzle walls. The 1 mm diameter injector is located 126 mm downstream of the fin leading edge and inclined at a  $45^\circ$  deg relative to the axial flow direction. As shown in Fig. 3b, the fin can be translated in the model Y axis which allows for different vortex injection locations to be examined.

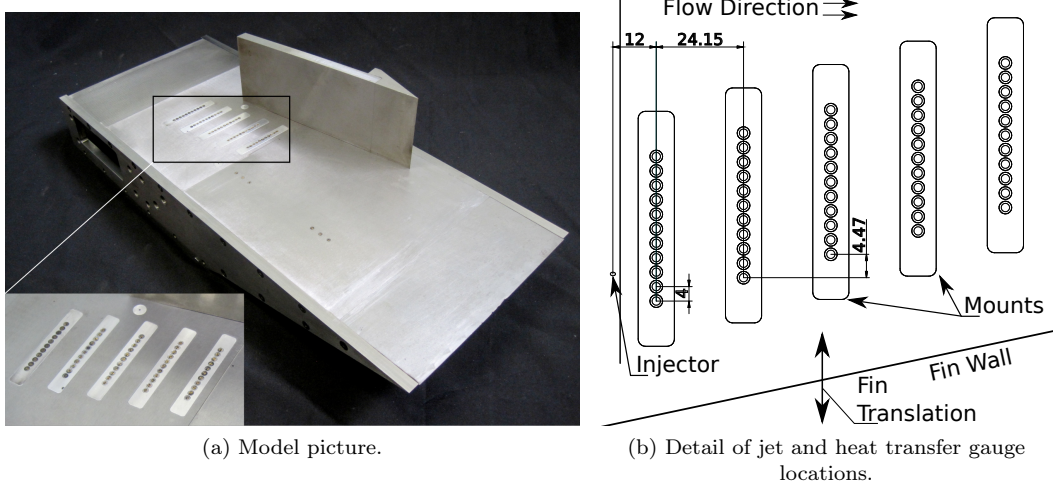


Fig. 3: Experimental model for measuring jet-vortex induced heat transfer.

*COMMENT IJ: The model Y direction is not defined. Add axis arrows to the figure*

The Thin-Film Heat-transfer Gauges (TFHG) in the model are arranged in five parallel lines as shown in Fig. 3b. Each of the gauge lines contains 11 TFHGs that were manufactured at the Centre for Hypersonics. These gauges consist of a  $\approx 20$  nm thick nickel resistive strip element that is sputtered onto an optically smooth quartz substrate. Shielded with a layer of  $SiO_2$ , the gauges are individually calibrated after manufacturing [13]. Once mounted into the experimental model, the heat flux can be calculated using the integrated measured change in the TFHG voltage from a constant current circuit using Eq. 1, from [13, 19], where  $\rho c k_T$  is the properties of the substrate and  $\alpha_R$  is the resistance-independent calibrated TFHG sensitivity.

$$\dot{q}_n = \frac{\sqrt{\rho c k_T}}{\sqrt{\pi} \alpha_R V_0} \sum_{i=1}^n \frac{V(t_0) - V(t_{i-1})}{(t_n - t_i)^{1/2} + (t_n - t_{i-1})^{1/2}} \quad (1)$$

Figure 3b also shows the TFHG sensor field that is required to appropriately resolve the heat-transfer profile across the injection-vortex interaction. The gauges centers are separated by 4 mm in the Y direction, while the lines are separated by 24 mm in the X direction (or freestream direction). Moreover, the gauge lines have a 4.5 mm offset in the positive Y direction in order to improve the sensor coverage. The first TFHG line is 12 mm downstream of the injector.

Additionally, the model incorporates six TFHG on the opposite side of the flat plate to the fin as shown in Fig. 3a. *COMMENT IJ: It is impossible to see the gauges in Fig 3a. I think it would be good to add a call-out with arrow pointing at gauges.*

These gauges are used to measure and identify the state of the undisturbed boundary layer in the vicinity of the fin leading edge and injection location. These gauges are grouped in two sets of three, 10 mm apart with the first set starting at 143 mm from the flat plate leading edge. This first group is centered at the same axial location as the fin leading edge to determine if the BL is laminar before the start of the vortex. The second set of gauges starts 249 mm downstream of the flat plate leading edge and is located just upstream of the injector. Both sets of gauges are located far enough away from the fin that there is no chance that the resulting oblique shock-wave and vortex can influence the data. The boundary layer was found to remain laminar for all test conditions presented in this paper.

Two pressure taps mounted flush with the flat plate surface incorporating kulite pressure transducers are used to measure the free-stream static pressure during the experiment.

#### A. T4 test flow conditions

The experiments were performed using the T4 Mach 7.6 nozzle at a Mach 8 flight-enthalpy. The nozzle exit flow conditions are derived from measurements of the shock tube fill pressure ( $P_{ST}$ ), shock tube shock-speed ( $u_S$ ), shock tube temperature ( $T_{ST}$ ), and the stagnation region nozzle supply pressure ( $P_e$ ). Shown in Table 1 are the calculated nozzle exit values tabulated along with their uncertainties.

Table 1: Nominal conditions during testing a nozzle exit.

Variable	Value
$P_0$ [MPa]	$15.7 \pm 4.42\%$
$P_\infty$ [kPa]	$2.29 \pm 4.53\%$
$T_\infty$ [K]	$237 \pm 7.37\%$
$\rho_\infty$ [ $\text{kg m}^{-3}$ ]	$0.0335 \pm 6.97\%$
$u_\infty$ [ $\text{m s}^{-1}$ ]	$2340 \pm 2.98\%$
$M_\infty$ [-]	$7.57 \pm 0.70\%$
$H_0$ [ $\text{MJ kg}^{-1}$ ]	$2.73 \pm 7.10\%$

The nozzle exit conditions in Table 1 are calculated using the in-house code NENZFr from the

University of Queensland [20]. NENZFr is a wrapper that integrates an ESTCj([ref]) shock-tube simulation into a space-marched thermal and chemical non-equilibrium Eilmer3 CFD simulation of the nozzle. Eilmer3 is a collection of programs for the simulation of 2-D/3-D thermal and chemical non-equilibrium transient flows, developed at the University of Queensland [21, 22].

The axisymmetric grid used for the space-marched Eilmer3 simulation is constructed by inscribing a uniform structured grid between a Bezier curve defining the nozzle wall and the nozzle centerline. The mesh employed in this study consisted of 600 by 40 elements in the axial and radial directions respectively. The chemical composition of the gas is calculated using finite-rate reactions with a five species air model:  $N_2$ ,  $O_2$ ,  $NO$ ,  $N$  and  $O$ . The thermodynamic properties are obtained using NASA CEA2 [21, 23].

Moreover, to improve the accuracy of the nozzle exit conditions an iterative approach is applied to determine the transition location in the nozzle. The baseline predictive value is iterated until a satisfactory solution is found that agrees with the experimentally measured static pressure on the model plate. The uncertainty of this measurement is lower than the resultant sensitivity from the nozzle transition location, and thus is considered a truth value target for the iterative convergence[7].

#### IV. Test cases

Two fin locations along the model Y axis were examined in the experimental campaign. Moving the fin adjusts the relative position between the jet and vortex and allows the effect of the effusing fluid on the resulting flowfield to be investigated. The fin locations are defined by the distance between jet and fin in the Y direction, non-dimensionalized by the jet diameter. The tested fin-to-injector distance ratios are  $26.2\phi_{inj}$  and  $35.2\phi_{inj}$ , and are named the Upper Fin (UF), and Lower Fin (LF) test cases respectively.

The initial tests case use No Injection (NI) and is used to obtain baseline heat flux data corresponding to an undisturbed vortex. For the jet-vortex interaction tests hydrogen is injected at two different plenum pressures at both fin locations. The tested pressures were  $P_{inj} = 1300 \text{ kPa}$  and  $P_{inj} = 430 \text{ kPa}$  and are named High Injection (HI) and Low Injection (LI) respectively. These two pressures produce injection-to-free-stream momentum ratios of 5.24, and 1.73. The plenum is fed

by a Ludwieg tube used in order to maintain a constant total pressure in the plenum.

All of these parameters were combined to produce six different test cases as summarized in Table 2.

Table 2: Combination of injection pressure and fin position for the different test cases.

# Naming	Injection Pressure	Fin-to-injector distance ratio
1 NI-UF	- (-)	26.2
2 NI-LF	- (-)	35.2
3 HI-UF	1300 kPa $\pm 3.1\%$	26.2
4 LI-UF	430 kPa $\pm 2.8\%$	26.2
5 HI-LF	1300 kPa $\pm 3.1\%$	35.2
6 LI-LF	430 kPa $\pm 2.8\%$	35.2

## V. CFD reference results

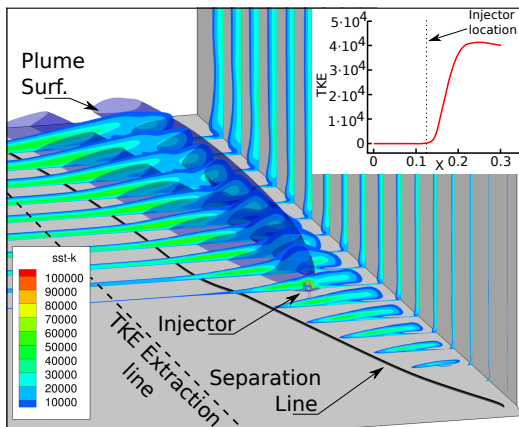
The data obtained in the experiments is complemented with numerical simulations to enhance the understanding of the results and assess the validity of the numerical methodology. The numerical domain spans from 10 mm upstream to 300 mm downstream of the fin leading edge and 200 mm centered around the injector centroid in the spanwise direction. The boundary layer development over the first 146 mm of the flat plate upstream of the fin leading edge was calculated in a separate quasi two-dimensional simulation with an infinitely sharp leading edge. The exit profile from this simulation is used as the inflow boundary condition for the three-dimensional numerical domain described above.

The structured three-dimensional domain contains approximately four million cells and has a minimum spacing in the vicinity of the injector of approximately 0.05 mm. The cell growth from the injector is restricted to 1 mm in the region of uniform flow and is considered an appropriate limit to resolve the far-field of the vortex-injection interaction. In the numerical domain, the injector is placed at  $X = 125$  mm, downstream from the fin leading edge and 26.2 and 35.2 fin-to-injector distances ratios from the fin in order to match the experiments. The walls are modelled as non-slip isothermal walls with a temperature of 300 K, the mean for the lab in which the experiments were conducted.

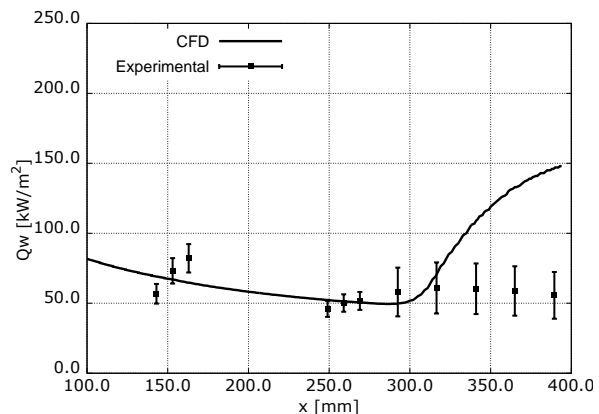
The inflow conditions used for the simulations are the nominal conditions calculated at the

nozzle exit in Table 1. Using the transition predictions for the T4 tunnel from He and Morgan [24], the plate was expected to stay fully laminar upstream of the oblique shock and injector. Thus, the pseudo-2D simulations to resolve the boundary layer development were conducted as fully laminar.

In the three-dimensional domain the RANS equations are closed with the SST  $k - \omega$  turbulence model. This ensures turbulent mixing of the fuel and the production of turbulence in the boundary layer region separated by the fin shock is correctly simulated. In order to accommodate the laminar inflow from the quasi-2D simulation, the Turbulent Kinetic Energy (TKE) at the inlet to the domain is set to zero. This replicates the laminar nature of the flow upstream of the fin, as seen in the experiments, for most of the flat plate. More importantly, using a zero TKE inflow with the SST  $k - \omega$  model, allows for an appropriate modeling of the viscous turbulence generation in the laminar boundary layer interacting with the fin shock and turbulence generation in the separations and injection-vortex interaction. The TKE generation along the *TKE Extraction line* shown in Fig. 4a is shown in the inset. Examining this trace of TKE in Fig. 4a, it is evident that TKE remains negligible in the initial part of the domain until a rapid increase just downstream of the injector. Thanks to the delayed onset of TKE growth, the flow relevant for the region of interest remains laminar until it separates, qualitatively representing the turbulent state of the flow in the experiments. Good agreement between the numerical and experimental results in the laminar region are further evident by comparing heat flux as shown in Fig. 4b.



(a) Turbulent kinetic energy (TKE) evolution in the numerical case.



(b) Experimental and numerical heat flux on the undisturbed flat plate region.

Fig. 4: Boundary layer state comparison between the experimental and numerical cases

## VI. Results

The experimental and numerical results for the six tests cases outlined in Table 2 are presented here. The no injection case is presented first to outline the baseline interaction followed by the vortex-injection cases and how these different scenarios influenced the flowfield.

### A. Unfueled vortex

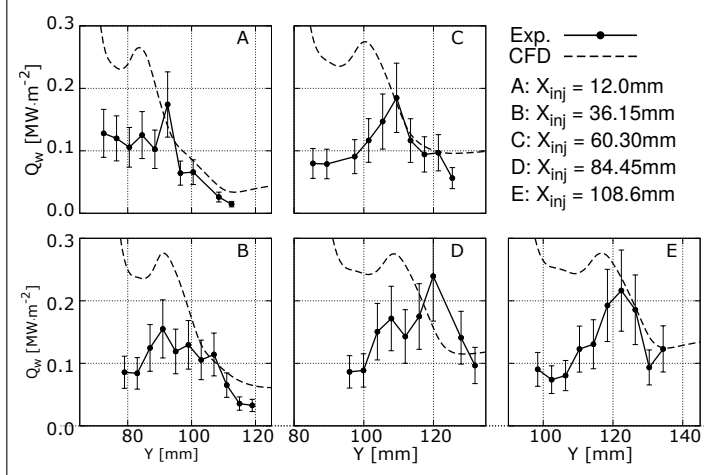
Two baseline cases using the UF and LF positions with no injection were investigated to identify the effect that the induced vortex had on the TFHGs in the experiment and to show how well the numerical methodology is able to accurately simulate the flowfield. Shown in Fig. 5 is the numerically predicted heat flux, extracted along transverse slices aligning with the TFHG inserts to allow for an accurate comparison between the two.

Subsets Fig. 5a and Fig. 5b correspond to the UF and LF positions respectively. For both cases, the further you traverse in the spanwise direction away from the oblique shock, the better the agreement. However, in the region closest to the fin (defined as low Y values), the heat flux is overestimated in the numerical results. This overestimation in the numerical data is consistent across the entire comparable domain, and it is visibly more prominent in the UF case. This fact is induced by the closer proximity of the fin to the TFHG in the UF case, placing more of the gauges inside the region of overpredicted heat transfer.

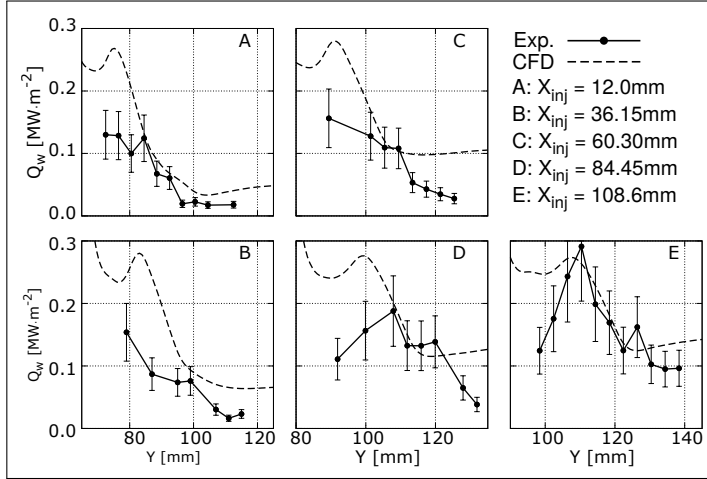
*COMMENT IJ: I think it would also be a good idea to draw attention to the error bounds of the TFHGs at this point. Error (or fluctuation with time) reduces further from the fin suggesting smoother and more regular flow.*

*KDB: No. The uncertainty on these readings should be propagated from the tunnel uncertainty limits, not taken as the two sigma Gaussian probability distribution. The uncertainty is based upon the mean taken during the test time and does not indicate smoother flow away from the fin, only that the heat flux is lower away from the vortex core/fin. You would have to measure the intermittency of the TFHG signals in order to make a statement about the level of turbulent/macro structures. I think those details would be outside the scope of this work.*

*Per your comment about the uncertainty calculation, I agree. There needs to be a sentence somewhere*



(a) Upper fin position.



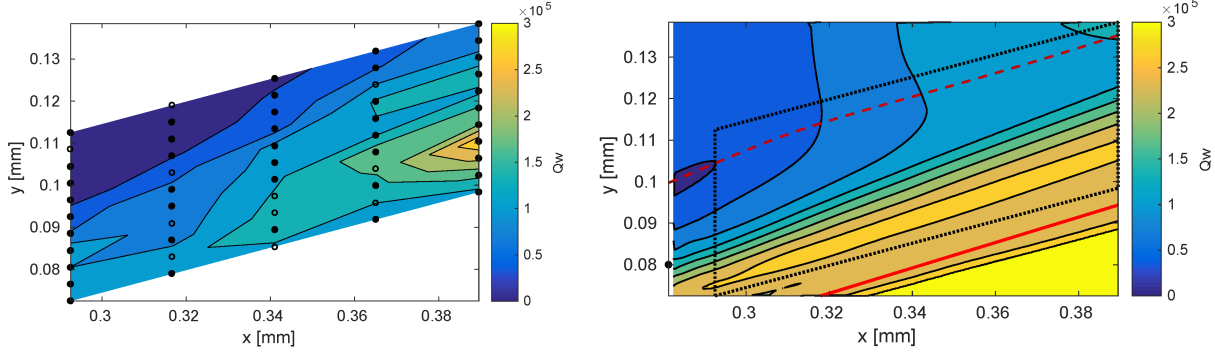
(b) Lower fin position.

Fig. 5: Numerical and experimental data on gauges lines A to E, at  $X_{inj}$  axial distance from the injector. Unfuelled vortex cases.

*about how it is calculated. You can just reference Dylan's thesis if you need a source Juan.*

Figure 6 presents an interpolated mapped version of the mean experimental data along with the equivalent numerical comparison for the LF case. In this position, the fin is placed further from the TFHGs and therefore, only a small part of the region with numerically overpredicted heat-flux falls within the measurement region. Also, shown on the figure are the vortex flowfield separation and reattachment lines. *COMMENT IJ: diagram doesn't show reattachment line you only have included extra lines for separation and fin shock.*

The reattachment takes place behind the fin shock, driving hot and dense shock compressed gas towards the flat plate, as labeled in Fig. 2b as 'jet'. This reattachment takes place in the region



(a) Experimental heat flux map. Solid dots are active gauges. Hollow dots are discarded gauges.  
(b) Numerical heat flux map. Dotted line indicates experimental acquisition area. Dashed red line indicates separation line. Solid red line indicates location of inviscid fin shock.

Fig. 6: Reconstructed heat transfer map. Comparison of heat flux from experiments and CFD. NI-LF (Case 2 in Table 2).

close to the fin where the numerical simulations over predict the heat flux. Assuming that the overall viscous shock process and flows are accurately modeled, the overestimation of heat flux can be attributed to an overestimation of the turbulence intensity in the region. This can be observed in Fig. 7, which shows a slice through the flow-field along line A from the UF case (Fig. 5a) combined with the TKE for the same axial location. The point where the numerical estimation begins to diverge from the experimental results, as shown on the figure, is coincident with a region of increased TKE immediately adjacent to the wall. The blown up image in Fig. 7 shows a better representation of the region of elevated TKE. Considering how numerical heat transfer is calculated, this high level of turbulence significantly enhances heat transfer, leading to the elevated values seen in the simulation data.

This discrepancy created by the numerical solver being unable to accurately simulate the heat flux near the fin shock is a key aspect to take into account when comparing the numerical and experimental data from the fueled results. This region of overestimation will be referred to as the ‘numerical overestimation zone’.

*COMMENT IJ: It would be good to finish off with a paragraph highlighting that overall agreement is good. I.e. that position of oblique shock is well captured and that heat transfer levels outside of shock are in good agreement. If you finish section as is, reader will be confused and doubt accuracy of experiment.*

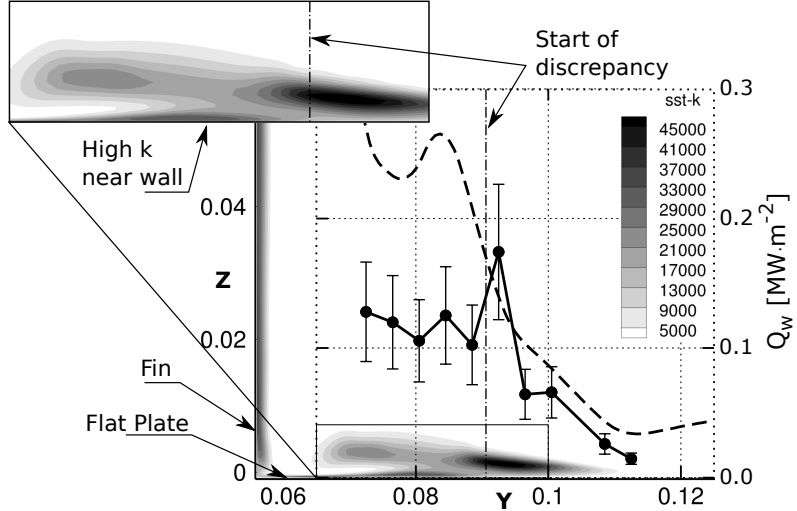


Fig. 7: Contours of turbulent kinetic energy combined with experimental and numerical heat flux data, along slice A (at  $X_{inj} = 12$  mm).

## B. Fuel vortex interaction

The results obtained for the tests using the UF and LF positions in combination with the high and low injection pressures (cases 3-6 in Table 2) provide data on the complex vortex-injection interaction flowfield.

### 1. Upper fin position, High injection pressure

The experimental and numerical results for the high injection pressure UF case are presented in Fig. 8. Qualitatively, there is a good agreement between the numerical and experimental results far away from the fin wall. The two curves have similar trends, and the heat flux peak induced by the injection bow shock is correctly simulated numerically. However, the numerical heat flux values near the fin (low Y values) are again overestimated when compared to the experimental results. This overestimation is caused by the presence of the ‘numerical overestimation zone’ previously outlined for the NI case.

*COMMENT IJ: It may be a good idea to comment on or introduce the doble peak seen at location A, as an artefact of the bow shock. Will help to build up understanding and appreciation of experimental data.*

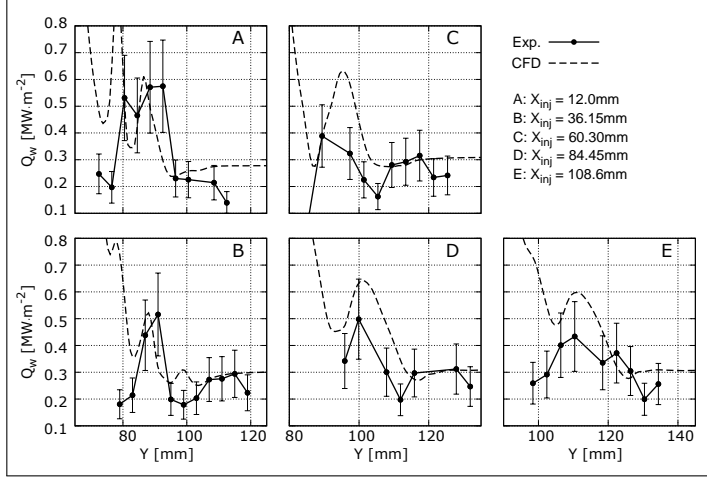
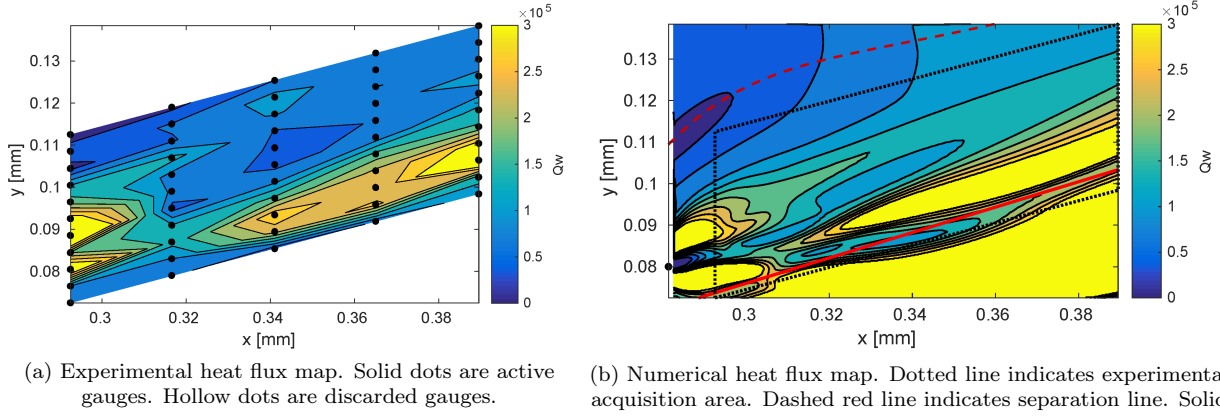


Fig. 8: Numerical and experimental heat transfer data. HI-UF (Case 1 in Table 2)



(a) Experimental heat flux map. Solid dots are active gauges. Hollow dots are discarded gauges.

(b) Numerical heat flux map. Dotted line indicates experimental acquisition area. Dashed red line indicates separation line. Solid red line indicates location of inviscid fin shock.

Fig. 9: Reconstructed heat transfer map. Comparison of heat flux from experiments and CFD. HI-UF (Case 3 in Table 2)

## 2. Flowfield description from numerical data

The numerical solution presents an interesting heat flux distribution on the flat plate consisting of a strip of elevated heat transfer running approximately longitudinally down the center of the vortex. This region extends from shortly downstream of the injection bow shock until beyond the experimental measurement area. This feature is difficult to visualize in Fig. 8, but is apparent in the heat flux maps shown in Fig. 9. This elevated strip is bracketed by the neighboring low heat flux strips, both highlighted in Fig. 10. Where Fig. 10 presents the three-dimensional numerical data showing the vortex-injection interaction.

Figure 10a displays the evolution of the flow from upstream of the injector until far downstream

of the injection. The fuel plume begins with a nearly hemispheric shape and evolves to a highly elongated profile. *COMMENT IJ: I think it would be to add a sentence cross-referencing to your paper describing the vortex flow structure.*

Far downstream, the fuel plume splits into two regions, one located within the vortex recirculation region, and the other adjacent to the flat plate wall (further from the fin than the vortex). This region of interest is presented in more detail in Fig. 10b. In this figure, the streak lines on the flat plate surface show that the high and low heat flux strips are coincident with the separation and reattachment of the flow. These reattachment and separation stream lines are linked to a counter rotating vortex shown in in Fig. 10c, marked as ‘C.R. vortex’.

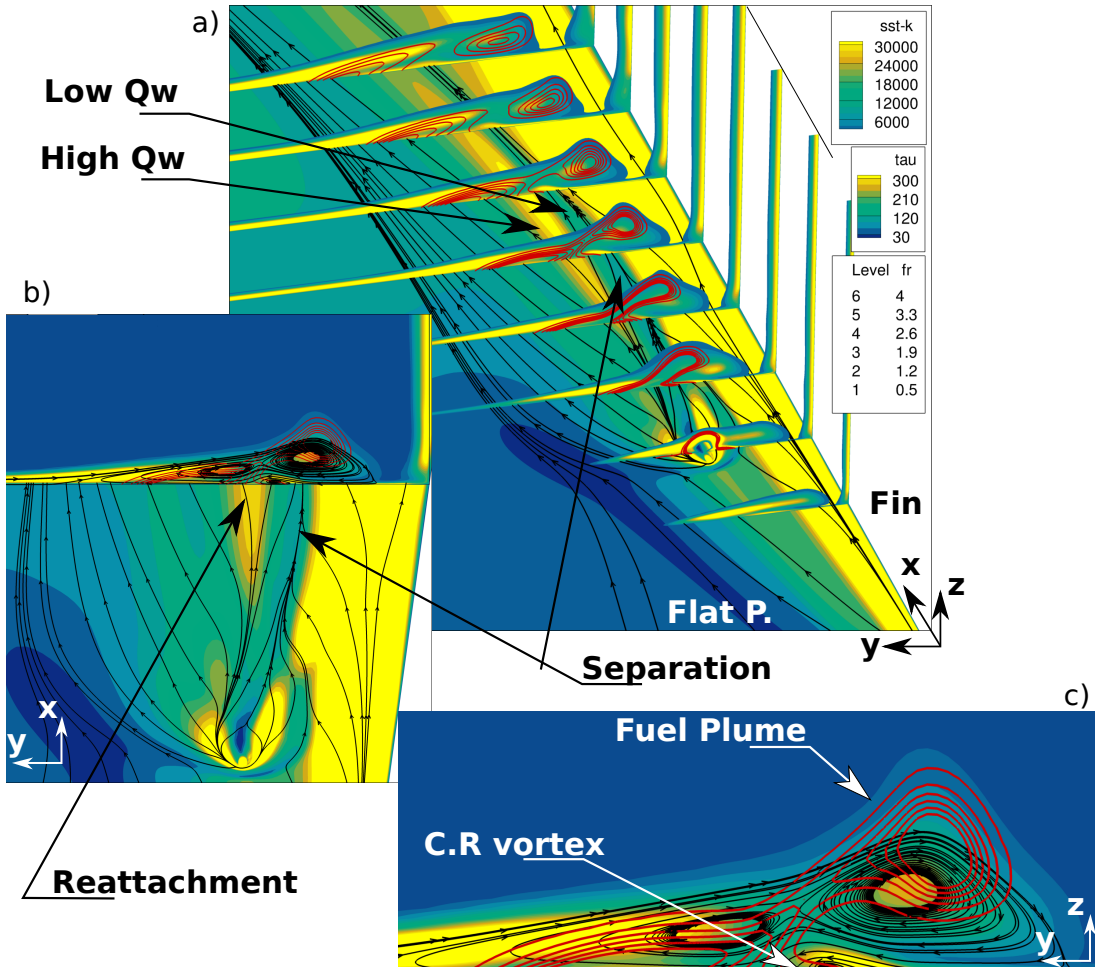


Fig. 10: Flat plate surface: numerical heat flux map with streak-lines. Slices: contours of turbulent kinetic energy, lines of equivalence ratio (red), and surface streamtraces. LP-HI-UF case.

Despite the heat flux overestimation by CFD close to the fin (as shown for the NI case), the ability of the numerical method to accurately predict the location and extent of the counter-rotating

vortex within the main separation indicates that the macro structures of the 3D flowfield are correctly modeled.

*COMMENT IJ: I think Figure 10, could be discussed in a bit more detail. It includes a lot of good information, that you don't go into (e.g. wall shear stress, macroscopic streaklines, etc...).*

*Finally, I think you may want to change the order of section VI.B.1 and 2. I.e. something like:*

- talk about interaction flow being a lot more complex
- explain the full flow field and what is going on using the CFD results (use current discussion that goes with Fig 10).
- Using numerical results, point out critical (measured) features that can be used to assess the correctness of your simulation
- Introduce and compare experimental results. These will reaffirm that certain key features are in good agreement between experiment and simulation.

### 3. Upper fin position, Low injection pressure

The LI-UF case has similar results to the HI-UF case. Shown in Fig. 11, the heat flux peaks are again well predicted and the region away from the fin shock resulted in a good agreement. Despite these similarities, the low injection case exhibits a larger discrepancy between the numerical and experimental data in the ‘numerical overestimation zone’.

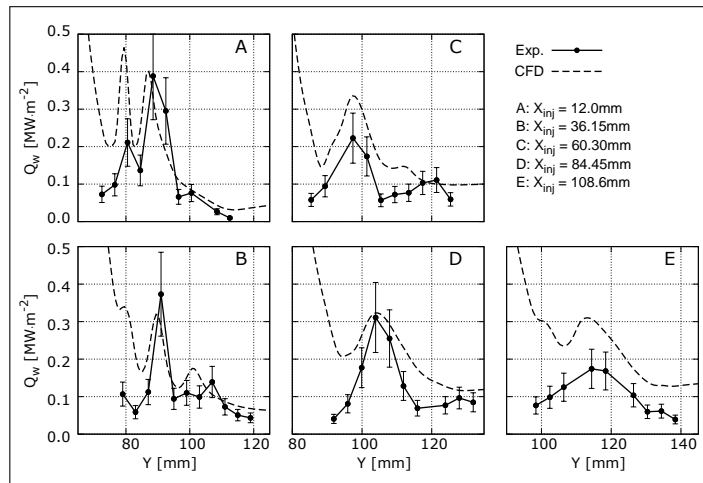


Fig. 11: Numerical and experimental heat transfer data. LI-UF (Case 2 in Table 2)

For the HI-UF, the injection bow shock has a larger influence the on heat flux, helping to decrease

the level of intrinsic error experienced from the ‘numerical overestimation zone’. *COMMENT IJ:*

*This link isn’t immediately obvious. Please elaborate and explain.*

In the LI-UF case shown in Fig. 11, the lower injection pressure makes the numerical error in the ‘numerical overestimation zone’ more influential on the final results. This is especially true in lines A and E. In Line A, the left peak is clearly overestimated due to its proximity to the fin and in Line E, the effect of the injection bow shock is largely dissipated, again increasing the relative effect of the ‘numerical overestimation zone’.

*COMMENT IJ: Include at least 1 sentence pointing out the parts that agree well. I think you can also elaborate a bit more on the bow shock effect. Comparing Fig 8 and 11, E it is clear that experimental heat flux in Fig 11 is about 1/3. Rather than having a purely qualitative argument, it would be good to include some quantitative parameters and to back these up with quantitative data from CFD. E.g. how much does density behind shock change between LI ad HI? How does the TKE close to the wall change between the two cases?*

#### 4. Lower fin position, High injection pressure

The heat flux results for the high injection pressure, low fin position (HI-LF) are presented in Fig. 12. These lines show a better agreement than the previous cases across the entire domain. In this case the fin shock is further from the injection location. Thus, the ‘numerical overestimation zone’ is further away from the region of interest and predicted heat flux better matches the experimental data, in particular close to the fin (low Y). This improvement in the correlation between the two results is particularly visible for Line A, where the two distinct heat flux peaks, created by the bow shock are clearly visible. This improved correlation increases the confidence in both the simulation and numerical results even though previous discrepancies were observed.

*COMMENT IJ: Be more positive. Talk about the features that agree well. I.e. explicitly mention good agreement for ALL lines, etc... This case is a very good result, but this is not clear from discussion.*

*Also you should make a stronger argument how this the good agreement gives you confidence for the earlier simulation. I.e. by being able to correctly predict all the flow features when you are further*

away from the over-estimation zone, this confirms that the numerical approach is sound.

The current single sentence gets lost...

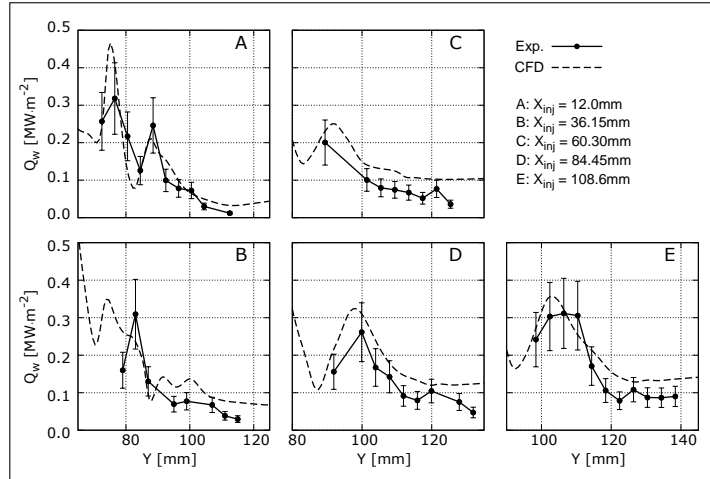


Fig. 12: Numerical and experimental heat transfer data. HI-LF (Case 3 in Table 2)

##### 5. Lower fin position, Low injection pressure

The LI-LF heat flux data is presented in Fig. 13. Again, thanks to the fin shock sitting being further away from the region of interest, the effect of the ‘numerical overestimation zone’ is reduced when compared to the LI-HF case. Nevertheless, the accuracy of the numerical method is lower than for the equivalent fin position with the higher injection rate (HI-LF). Similar to the difference shown for the UF cases, this decrease in the accuracy is caused by the reduced effect of the injection bow shock on the measured heat flux values.

*COMMENT IJ: You need to rephrase the last two sentences. They kind of contradict. In the first you say that numerical simualtion is less accurate (i.e. has larger inherent error) then you say the error is caused by weaker bow shock.*

*Revise in line with previous comments.*

## VII. Conclusions

A canonical geometry consisting of a flat plate plus a fin with a compression angle has been used to generate vortices representative of those intrinsically generated by scramjet inlets. By injecting within this vortex, the vortex-injection interaction and its effect on the heat flux was able to be

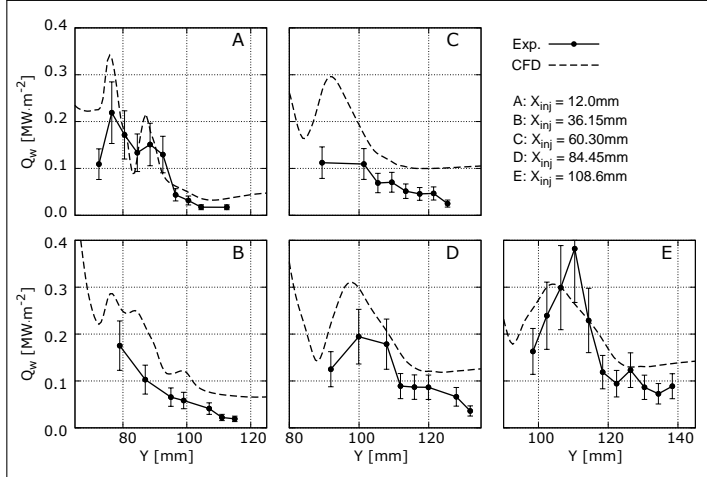


Fig. 13: Numerical and experimental heat transfer data. LI-LF (Case 4 in Table 2)

studied. Both numerical and experimental results were obtained allowing for the validity of the numerical methodology to accurately predict the experimental results to be assessed.

The vortex measurements with no injection showed a localized region of severe discrepancy near the fin wall between the experimental and numerical results. This limitation of the numerical methodology was identified as a tendency of the  $SSTk - \omega$  turbulence model to overpredict the turbulent intensity on the flat plate surface near the fin. This overestimation of the turbulence intensity was also shown to influence the numerical results for the fueled cases as well. The effect was found to be less severe as the fin was translated away from the experimental data acquisition gauges.

Despite the limitations of the numerical methodology due to the localized overestimated heat flux, the location of the injection bow shock and secondary counter-rotating vortex was able to be accurately predicted. Moreover, the correlation between the numerical and experimental results in general increased as you moved in the transverse direction away from the fin. This increased correlation suggests the that the numerical methodology was able to accurately predict the flow structure but needs improvement in the fin shock separation region adjacent to the wall for both the fueled and unfueled scenarios.

## VIII. Bibliography

- [1] Smart, M. K. & Tetlow, M. R., *Orbital delivery of small payloads using hypersonic airbreathing propulsion*, J. Spacecraft Rockets, **46**, No.1, 2009, 117-125.
- [2] Cook, S. & Hueter, U., *NASA's integrated space transportation plan 3rd generation reusable launch vehicle technology update*, Acta Astronautica, 53, 2003, 719-728.
- [3] Alvi, F. S. & Settles, G. S., *Physical model of the swept shock wave/boundary-layer interaction flowfield*, AIAA Journal, 30, No.9, 1992, 2252-2258.
- [4] Llobet, J. R., Jahn, I. H. & Gollan, R. J., *Effect of stream-wise Vortices on Scramjets Porthole Injection Mixing*, Proceedings for the 20th AIAA International Space Planes and Hypersonic Systems and Technologies Conference, Glasgow, 2015.
- [5] Llobet, J. R., Gollan, R. J., & Jahn, I. H., *Scramjet inlet vortices: its effect on fuel plume elongation and mixing rate*, publication pending.
- [6] Llobet, J. R., Barth, J. E. & Jahn, I. H., *Vortex Tracking Algorithm for Hypersonic Flow in Scramjets*, 19th AFMC, 8-11 December, Melbourne 2014. Submitted for publication.
- [7] Doherty, L. J. (2013). Experimental Investigation of an Airframe Integrated 3-D Scramjet at a Mach 10 Flight Condition. University of Queensland.
- [8] Stalker, R .J., *The Free-Pison Shock Tube*, The Aeronautical Quarterly, 1966, 351-370.
- [9] Tanimizu, K. (2008). Nozzle Optimization Study and Measurements for a Quasi-Axisymmetric Scramjet Model. University of Queensland.
- [10] Kirchhartz, R. M. (2009). Upstream Wall Layer Effects on Drag Reduction with Boundary Layer Combustion. University of Queensland.
- [11] Ridings, A. N. (2015). Investigation of pre-combustion shock trains in a scramjet using a shock tunnel at Mach 8 flight conditions. The University of Queensland, School of Mechanical and Mining Engineering.
- [12] Khang, W. C. Y. (2012). Effects of flow non-uniformities on the drag reduction by boundary layer combustion, (August).
- [13] Wise, D., *Experimental Investigation of a 3D Scramjet Engine at Hypervelocity Conditions*, PhD thesis, The University of Queensland, 2014.
- [14] Stalker, R. J., Paull, A., Mee, D. J., Morgan, R. G., & Jacobs, P. A. (2005). Scramjets and shock tunnels -The Queensland experience. Progress in Aerospace Sciences, 41, 471â€“513.
- [15] Itoh, K., Ueda, S., Komuro, T., Sato, K., Tanno, H., & Takahashi, M. (1999). Hypervelocity aerothermodynamic and propulsion research using a high enthalpy shock tunnel Hiest. In 9th International Space Planes and Hypersonic Systems and Technologies Conference.

- [16] Wise, D. J., & Smart, M. K. (2014). Roughness-Induced Transition of Hypervelocity Boundary Layers. *Journal of Spacecraft and Rockets*, 51(3), 847–854. <https://doi.org/10.2514/1.A32674>
- [17] Hunt, D. C., Paull, A., Boyce, R. R., & Hagenmaier, M. (2009). Investigation of an Axisymmetric Scramjet Configuration Utilising Inlet Injection and Radical Farming. In 19th International Symposium on Airbreathing Engines (ISABE2009).
- [18] Llobet, J. R., Jahn, I. H. & Gollan, R. J., *Effect of vortex-injection interaction on wall heat transfer in a flat plate with fin corner geometry*, Trans. JSASS Aerospace Tech. Japan, Vol.15, No.APISAT-2016, 2017, a17-a26.
- [19] Schultz, D. & Jones, T., *Heat-Transfer Measurements in Short-Duration Hypersonic Facilities*, AGARD-AG-165, North Atlantic Treaty Organization Advisory Group for Aerospace Research and Development, 1973.
- [20] Doherty, L., Zander, F. , Jacobs, P., Gollan, R., Chan, W., & Kirchhartz, R., *NENZF-r: Non-Equilibrium Nozzle Flow, Reloaded. A User Guide.*, Mechanical Engineering Report 2012/08, The University of Queensland School of Mechanical and Mining Engineering, 2012.
- [21] P. A. Jacobs, R. J. Gollan, A. J. Denman, B. T. O'Flaherty, D. F. Potter, P. J. Petrie-Repar, & I. A. Johnston., *Eilmer's Theory Book: Basic Models for Gas Dynamics and Thermochemistry.*, Mechanical Engineering Report 2010/09, The University of Queensland School of Mechanical and Mining Engineering, 2010.
- [22] P. A. Jacobs, & R. J. Gollan., *The Eilmer3 Code: User Guide and Example Book.*, Mechanical Engineering Report 2008/07, The University of Queensland School of Mechanical and Mining Engineering, 2009.
- [23] McBride, B. J., & Gordon, S., *Computer program for calculation of complex chemical equilibrium compositions and applications. Part 2: User manual and program description.*, Reference Publication 1311, NASA, 1996.
- [24] He, Y. & Morgan, R. G., *Transition of compressible high enthalpy boundary layer flow over a flat plate*, Aeronautical Journal, 98(972), 2534.